用于产生红外脉冲的碲烯纳米片的化学气相输运生长

庞修洋[1]，赵新新[2]，俞强[1*]，邓海芹[1]，刘方奇[3]，张严[2]，殳博王[1]，贤天浩[4]，朱思聪[3]，吴坚[1]，侯义锋[5]，张凯[2**]，姜宗福[1]

[1]国防科技大学前沿交叉学科学院，脉冲功率激光技术国家重点实验室，高能激光技术湖南省重点实验室，湖南 长沙 410073；

[2]中国科学院苏州纳米技术与纳米仿生研究所，创新实验室，纳米器件与应用重点实验室，纳米光子材料与器件重点实验室，江苏 苏州 215123；

[3]武汉科技大学耐火材料和冶金学国家重点实验室，湖北 武汉 430081；

[4]上海交通大学物理与天文学院，上海 200240；

[5]梧州学院电子与信息工程学院，广西 梧州 543001

摘要 碲烯具有宽带吸收、高迁移率和独特的拓扑性质，在红外光学应用领域被寄予厚望。本团队利用化学气相输运方法制备了高结晶性碲烯纳米片；结合精准的端面转移技术，获得了利于光纤集成的可饱和吸收体；基于碲烯的非线性饱和吸收特性，在 1.55 μm 波段实现了稳定的被动调 Q 脉冲输出，中心波长约为 1558 nm，脉冲宽度约为 1.44 μs，重复频率在 87～133 kHz 范围内可调。本研究结果拓展了新型碲烯纳米材料的应用场景，为可调谐脉冲激光提供了解决方案。

关键词 激光器；纳米材料；可饱和吸收体；被动调 Q；可调谐脉冲激光；碲烯

1 引　言

脉冲光纤激光器具有结构紧凑、制作成本低、光束质量高等特点，在工业加工、生物成像、医学检测和精密测量等领域得到了广泛关注[1]。已有的脉冲光纤激光器主要通过被动锁模[2]和调 Q 技术实现激光输出，其中的调 Q 技术能够实现微秒至纳秒量级脉冲输出。调 Q 激光具有重复频率可调、脉冲能量高、易于放大等特点。可饱和吸收体被认为是产生超短脉冲激光的关键器件[3]。当入射光强超过一定阈值时，可饱和吸收体的透射率随入射光功率的增加而迅速变化，呈现出非线性吸收特性，可以被动地调制腔内损耗。

近年来，低维材料在光子学研究领域得到了长足发展[4]，近期报道的一些研究工作展现了其广阔的应用前景[5-9]。2009 年，石墨烯薄膜作为可饱和吸收体被首次应用于超快脉冲激光的开发。石墨烯具有低饱和强度、超快恢复时间、可变调制深度和宽带响应等优点[10]。2016 年，Loiko 等[11]报道了基于石墨烯的调 Q 掺铒光纤激光器。随后，越来越多的低维材料被开发并用作超快脉冲激光器的高效可饱和吸收体，例如拓扑绝缘体（TI）[12-13]、二维过渡金属硫族化合物（TMDs）[14-17]、黑磷（BP）[18]等。其中，低成本和环境稳定的单元素可饱和吸收材料是目前的研究热点。随着制备技术的进步，许多碳族、氮族、氧族单元素薄膜的制备得以实现，如砷[19]、锑[20-21]和碲[22]等。其中，碲烯是氧族元素中的一种基本材料，具有螺旋链结构，能够生长出纳米线、纳米棒、纳米管或纳米带等。2014 年，Wang 等[23]通过范德瓦耳斯外延方法生长出厚度为 30 nm、横向尺寸为 6～10 μm 的二维六边形碲纳米片，该纳米片表现出了良好的光响应性能。2018 年，Wang 等[24]基于溶液法生长了厚度可调的二维碲纳米片，并用其制备了场效应晶体管，实验结果显示，该二维碲纳米片具有优异的电学性能和环境稳定性。2019 年，Guo 等[25]先通过液相方法制备碲纳米片，再将碲纳米片与聚乙烯吡咯烷酮（PVP）混合得到 Te/PVP 膜；测试结果显示，该 Te/PVP 膜在 800～1550 nm 范围内的非线性吸收系数约为 10^{-1} cm/GW，且具有高效的宽带饱和吸收能力。Guo 等将制备的 Te/PVP 膜作为可饱和吸收体，在通信波段获得了 829 fs 的高稳定飞秒脉冲。2021 年，Liu 等[26]同样采用液相法从碲块体中剥离出碲纳米片，然后利用双臂检测技术表征了碲纳米片的低饱和强度（1.06 MW/cm²）和高调制深度（35.64%）；他们将剥离出的碲纳米片作为可饱和吸收体，在 1558.8 nm 波段实现了皮秒（1.03 ps）脉冲。

综上，碲烯在光电子学领域具有较大的发展潜力[27]。本团队前期系统地研究过碲烯单晶的二次谐波（SHG）性能，结果显示，碲烯纳米片是潜在的倍频晶体[22]。然而，基于碲烯的时域可调脉冲光纤激光器还有待进一步研究。

本团队采用化学气相传输法（CVT）成功制备出了碲烯纳米片，其厚度约几十纳米，横向尺寸最大为 80 μm，对该碲烯纳米片进行物理化学表征后发现其具有较高的晶体质量；采用精准转移技术得到光纤端面集成的可饱和吸收体；基于碲烯的非线性特性，在通信波段（1.55 μm）实现了稳定的被动调 Q 脉冲输出，中心波长约为 1558 nm，脉冲宽度约为 1.44 μs，重复频率在 87～133 kHz 范围内可调。本研究工作展示了碲烯纳米片在超短脉冲激光器中的应用前景，可进一步改进二维单质材料的可控制备并推动其在超快光子学应用方面的发展。

2 碲烯可饱和吸收体的制备与表征

通常，二维材料的制备分为自上而下和自下而上两种途径，其中自上而下的途径相对比较简单。自上而下的方法主要有机械剥离法和溶液法。机械剥离法可以从单晶块材中剥离出质量较高的二维薄膜，但是不易控制薄膜的形状和厚度，而且难以大规模制备；溶液法也是获得纳米片的常用方法，但其也有不足之处，如容易引入有机杂质，有时会使晶体产生缺陷。自下而上的方法主要有物理气相沉积法（PVD）和化学气相传输法[28]。本次实验选用化学气相传输法制备碲烯纳米片，这种方法常被用来制备高结晶质量的块材。近几年，本团队已采用化学气相传输法成功合成了高质量的二元材料 TaS_2 和三元材料 $MnPSe_3$[29-30]。

样品制备流程：1）将碲粉（10 mg，纯度为 99.99%）和云母衬底分别放在中部缩颈的石英管两端（石英管外径为 10 mm，内径为 8 mm），在负压（10^{-2} Pa）环境中密封石英管；2）将石英管放入设定好温度程序的 OTF-1200X 型双温区管式炉中，利用原料端和沉积端之间的温度梯度（原料端温度为 450 ℃，沉积端温度为 350 ℃）实现汽化、输运和沉积结晶等过程；3）经过 30 min 的生长后，自然冷却至室温。

这里需要说明以下三点：1）将碲粉和衬底封闭在石英管中可以很好地避免氧气和其他环境因素的干扰，仅依靠温度和原料添加量来调节碲烯纳米片的生长行为；2）因为碲的熔点低，易于蒸发和运输，所以在其生长过程中并没有添加运输剂来辅助其生长；3）样品制备流程中的工艺条件对碲烯生长行为的影响很大，相关信息可参考文献[22]。

图 1（a）、（b）、（c）是碲的原子结构模型，碲原子通过沿 c 轴的共价键连接形成螺旋链，其他方向通过范德瓦耳斯力结合，排列成六边形结构。材料更倾向于沿纵向生长，因为沿横向生长需要更多能量。温度的设定至关重要，温度梯度决定着石英管中的
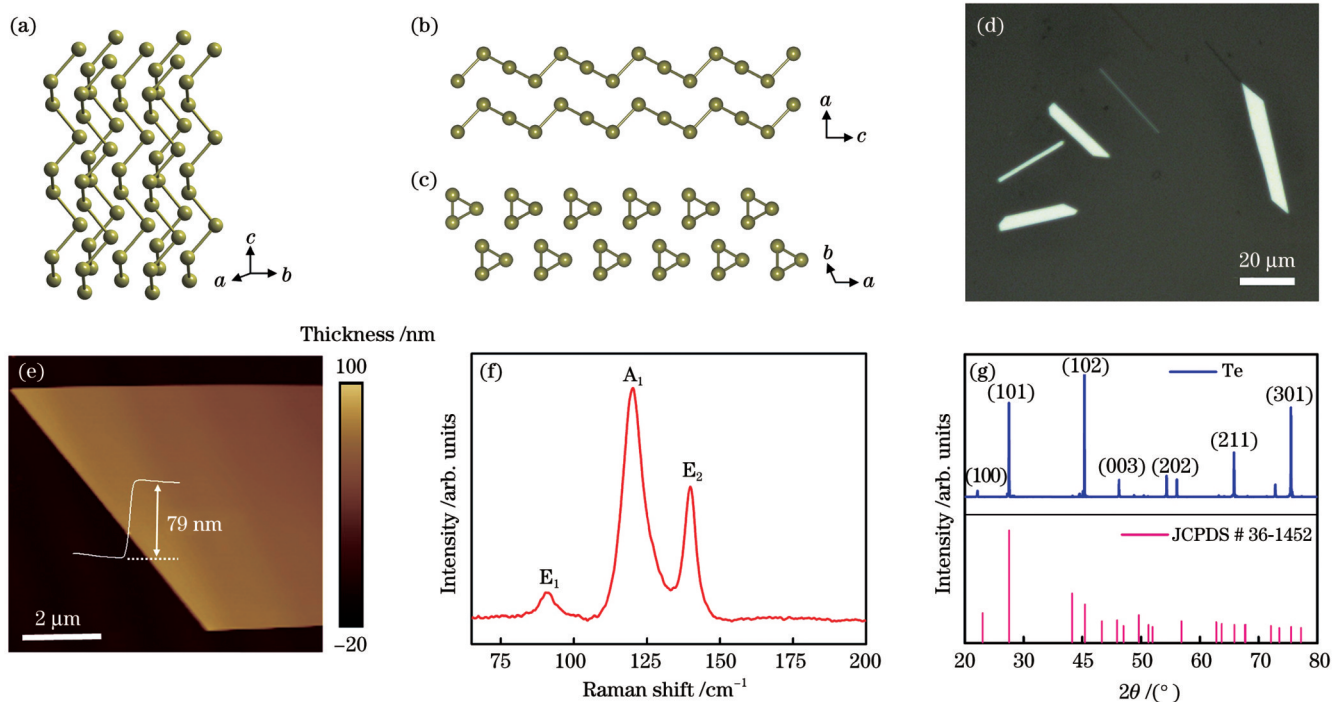

图 1 碲烯纳米片的结构与表征。(a)～(c)不同方向观察的原子结构模型；(d)碲烯纳米片的 OM 图像；(e)碲烯纳米片的 AFM 表征；(f)碲烯纳米片的拉曼光谱；(g)碲烯纳米片的 XRD 谱

Fig. 1 Structure and characterization of Te nanoflakes. (a)–(c) Atomic structural model of Te viewed in different directions; (d) OM (optical microscopy) image of Te nanoflakes; (e) AFM (atomic force microscopy) image of Te nanoflake; (f) Raman spectrum of Te nanoflake; (g) XRD (X-ray diffraction) spectra of Te nanoflake

蒸气压力。在合适的沉积端温度(350~380 ℃)范围内,碲原子可以克服迁移的能垒,加快向衬底的迁移速率。此外,云母衬底光滑的表面有利于原子在衬底上迁移。当能量达到横向生长所需的能量时,碲原子可以沿着平行于衬底的多个方向外延生长,最终形成二维纳米片[30]。当原料端温度保持不变而沉积端温度升高到 350 ℃时,即可在云母衬底上获得碲烯纳米片。

采用光学显微镜(OM)表征碲烯纳米片的形貌。如图1(d)所示,碲烯纳米片呈长条状,显示出浅金属色,其长度可达 80 μm,宽度为 20 μm。采用原子力显微镜(AFM)表征碲烯纳米片的厚度,结果显示其厚度约为 79 nm。如图1(e)所示,纳米片表面均匀,没有明显的起伏。使用激光共聚焦拉曼光谱仪(RAMAN)表征碲烯纳米片的拉曼光谱,结果如图1(f)所示,在 92、120、140 cm^{-1} 处有三个振动峰,分别对应于碲的 E$_1$(横向 TO 模式)、A$_1$ 和 E$_2$ 活性拉曼声子模式,与之前报道的典型特征峰[22]相符。采用 X 射线衍射仪(XRD)对碲烯纳米片进行表征,衍射光谱如图1(g)所示。将碲烯纳米片的 XRD 谱与标准晶体学卡片(JCPDS♯36-1452)进行对比,结果显示特征晶面与标准晶体学卡片对应,说明制备的碲烯纳米片具有较高的结晶质量。

为了进一步表征碲烯纳米片的微观结构,采用透射电子显微镜(TEM)进行观察。如图2(a)所示,在低分辨成像下,纳米片呈典型的长条状,且伴随有明显的边角形貌。相应的高分辨率透射电子显微镜(HR-TEM)图像显示出了清晰的原子像,如图2(b)所示,图中标示出了两组正交晶面,晶面间距分别为 0.60 nm 和 0.39 nm,可以对应到(0001)晶面和(11$\bar{2}$0)晶面。图2(b)中的插图为选区电子衍射(SAED)花样,可见清晰且整齐的衍射斑点。图2(a)、(b)证实了碲烯纳米片的高结晶性。图2(c)所示的能量色散X射线光谱(EDS)显示碲烯纳米片样品主要由碲元素组成(铜信号源于铜网),说明制备的碲烯纳米片样品具有较高的纯度。
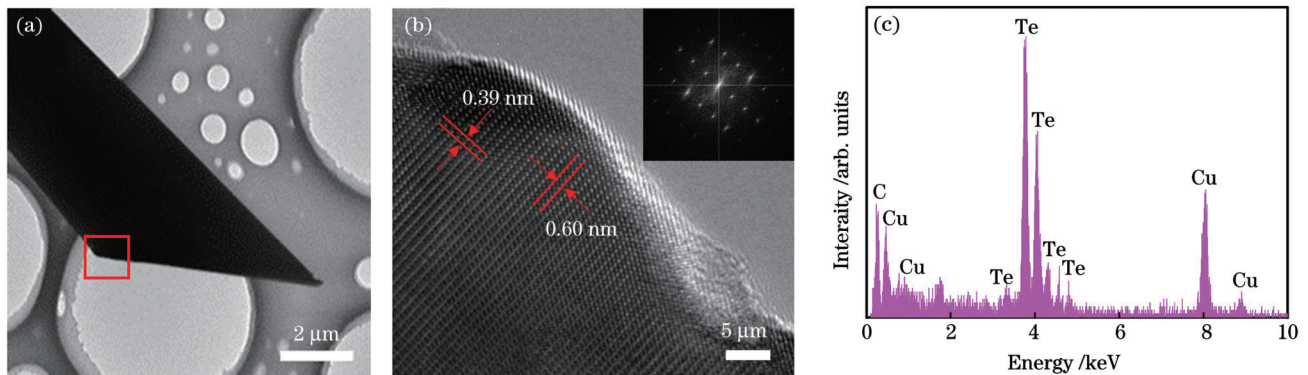

图 2 碲烯纳米片的精细结构及成分分析。(a)低分辨明场像;(b)高分辨像,插图为选区电子衍射花样;(c)EDS谱

Fig. 2 Fine structure and component analysis of Te nanoflake. (a) Low-magnification bright-field image; (b) high resolution image, where the insert shows selected area electron diffraction (SAED) pattern; (c) energy dispersive X-ray spectroscopy (EDS) spectrum

3 分析与讨论

基于图3(a)所示的双臂探测系统对碲烯纳米片的可饱和吸收特性进行测试[13]。首先,利用自建的三维转移平台,结合自制的聚二甲基硅氧烷(PDMS)薄膜将碲烯纳米片从云母衬底粘起;随后,将光纤端面固定在样品台上,将带有目标纳米片的 PDMS 膜固定在三轴悬臂梁上,慢慢靠近纤芯;缓慢控制纳米片和纤芯达到同一焦面,使薄膜紧贴光纤端面,然后缓慢提起 PDMS 膜,将碲烯纳米片留在纤芯位置。图3(b)是转移材料后的光纤端面,纤芯位置用圆圈标记,纤芯已被碲烯纳米片完全覆盖。双臂探测系统的光源是运行波长为 1550 nm 的脉冲激光,其重复频率为 16.6 MHz,脉冲宽度为 448 fs。通过耦合器(OC)将光信号分成两路,一路通过碲烯纳米片,另一路通过对应长度的光纤进行对照。分别测量两路光束的输出功率,并将其换算成可饱和吸收体的透射率。调节泵浦光源的功率密度,得到随泵浦功率密度变化的透射率数据,如图3(c)所示。透射率与泵浦光源功率密度的拟合曲线为

$$T(I) = 1 - \Delta T \times \exp\left(-\frac{I}{I_{sat}}\right) - T_{ns}, \quad (1)$$

式中:$T(I)$ 为透射率;ΔT 为调制深度;T_{ns} 为非饱和损耗;I_{sat} 为饱和光强;I 为光强。由拟合曲线可知,调制深度为 0.5%,饱和光强为 0.66 GW/cm^2,非饱和损耗为 99.16%。可见,碲烯纳米片表现出了较小的调制深度[31]。

基于碲烯可饱和吸收体构建图4所示的光纤激光环形腔,以验证其脉冲输出性能。环形腔的总长度约为 15 m,其中包括一段 3.2 m 长的掺铒光纤(Er110,6 μm/125 μm),掺铒光纤的色散系数为 28 ps^2/km。利用 980 nm/1550 nm 波分复用器(WDM)将泵浦激光
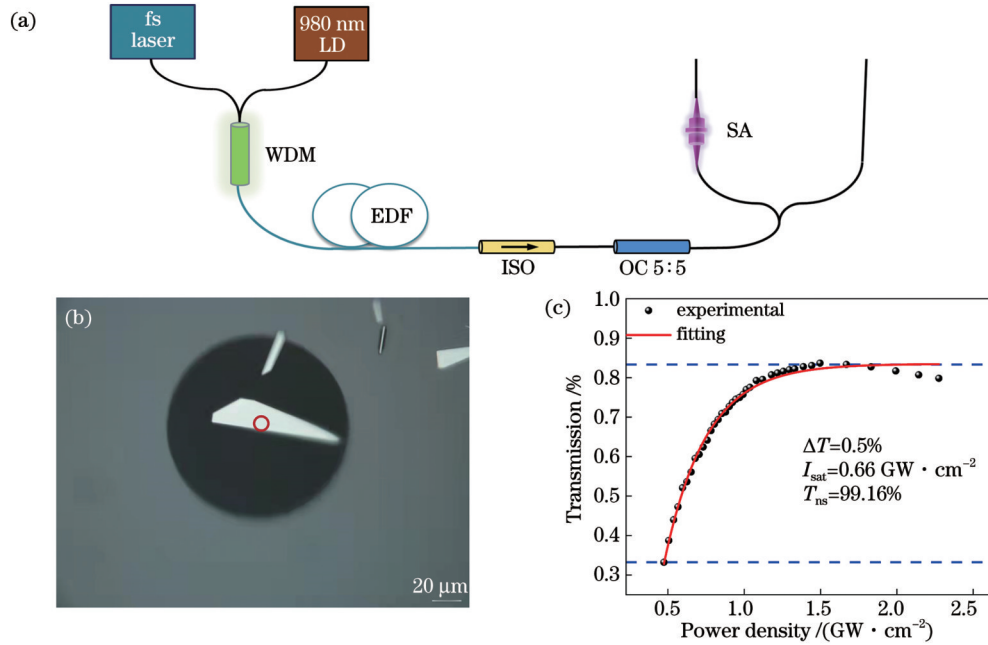
图 3　碲烯纳米片的非线性饱和吸收表征。(a)双臂探测装置示意图,其中,LD 表示激光二极管,WDM 代表波分复用器,EDF 代表掺铒光纤,ISO 代表光纤隔离器,OC 代表光耦合器,SA 代表可饱和吸收体;(b)光纤端面图;(c)可饱和吸收曲线图

Fig. 3　Nonlinear saturation absorption characterization of Te nanoflake. (a) Two-arm detection experimental device, where LD represents laser diode, WDM represents wavelength division multiplexing, EDF represents erbium-doped optical fiber, ISO represents isolator, OC represents optical coupler, and SA represents saturable absorber; (b) optical fiber end face; (c) saturable absorption curve
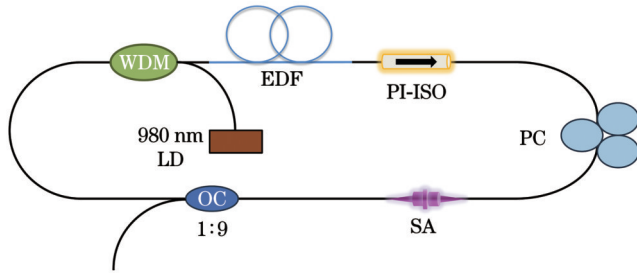

图 4　基于碲烯可饱和吸收体的脉冲光纤激光器示意图,其中 PI-ISO 表示偏振无关隔离器,PC 表示偏振控制器

Fig. 4　Schematic of pulse fiber laser based on Te saturable absorber, where PI-ISO represents polarization-insensitive isolator and PC represents polarization controller

(波长为 980 nm)耦合到环形腔中。采用偏振无关隔离器(PI-ISO)防止腔内反射,保证激光单向运行。利用偏振控制器(PC)调节振荡光束的偏振状态。采用光耦合器(50∶50)提取信号并用于脉冲监测。在光耦合器的输出端,一路光信号由光电探测器(2 GHz)转化为电信号,利用含射频分析功能的示波器(采样频率为 6 GHz)进行电信号的探测,记录其时域和频域特征;另一路光信号用光谱仪(最高分辨率为 0.02 nm,量程为 500~1700 nm)探测,记录输出激光的光谱特征。用功率计(量程为 5~500 mW)记录激光的输出功率。

在实验过程中,通过逐渐增大泵浦功率来寻找脉冲的启动阈值。起初,输出信号表现为连续激光输出;当泵浦功率增加到 50 mW 时,示波器上出现周期性脉冲序列,脉冲间隔随着激光功率增加而逐渐变大;当泵浦功率在 225~400 mW 范围内连续变化时,可以持续观测到被动调 Q 激光输出,如图 5(a)所示。在 225~400 mW 泵浦功率范围内,用光谱仪同时记录不同的输出光谱,如图 5(b)所示,中心波长稳定在 1558 nm 左右。调节泵浦功率为 300 mW,单独记录脉冲的时频特性,如图 5(c)所示。在 0~600 kHz 采样频率下记录的脉冲频谱如图 5(c)中的插图所示。进一步缩小采用频率范围为 0~150 kHz(分辨率为 100 Hz),频谱呈现为一个明显的单峰,脉冲的基频为 90.45 kHz,信噪比为 53.96 dB。这一结果表示输出脉冲具有良好的稳定性。图 5(d)是单个脉冲的拟合曲线,其脉冲宽度大约为 1.44 μs。

接下来进一步分析脉冲信号的特征。如图 6(a)所示,在 225~400 mW 泵浦功率范围内,脉冲宽度和重复频率随着泵浦功率的增加整体上呈现出相同的变化规律:随着泵浦功率增加,脉冲宽度呈现先下降后上升的趋势,且在 250~350 mW 区间内的变化较小;重复频率在 87~133 kHz 范围内可调,总体呈先下降后上升的趋势。由图 6(b)可知中心波长随着泵浦功率的增大而增大。这是因为掺铒光纤激光器的增益与泵浦功率密切相关,调节泵浦功率会改变腔内增益,最终导致波长红移,但波长的变化幅度在亚纳米量级。
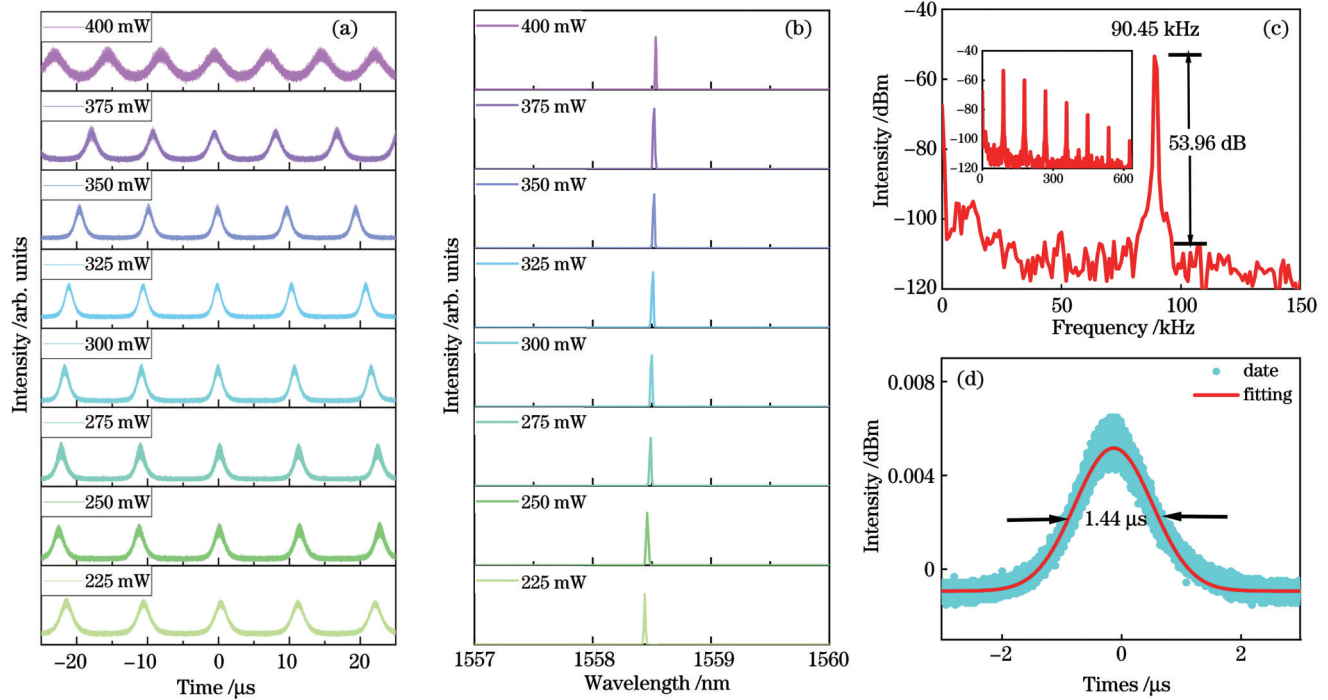
图 5　基于碲烯可饱和吸收体的脉冲激光的输出特性。(a)不同泵浦功率下的脉冲序列；(b)不同泵浦功率下的脉冲光谱；(c)特定泵浦功率下的频谱，插图为0～600 kHz频率范围内的射频频谱；(d)单个脉冲的拟合曲线

Fig. 5　Output characteristics of Te saturable absorber based pulse laser. (a) Pulse sequence at different values of pump power; (b) spectra at different values of pump power; (c) frequency spectrum at a particular pump power, where the insert is radio frequency spectrum in the frequency of 0–600 kHz; (d) fitting curve at single pulse
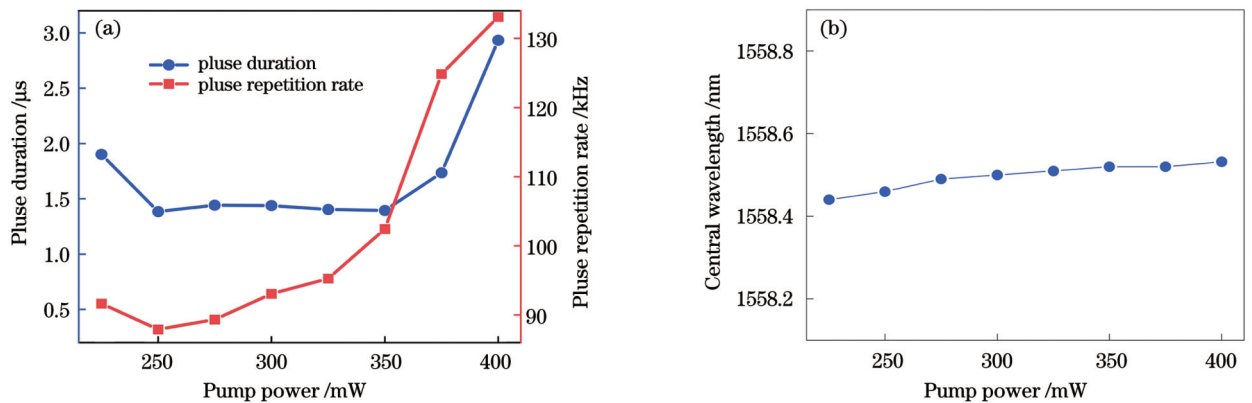

图 6　脉冲信号的变化趋势。(a)脉冲宽度和重复频率与泵浦功率的关系；(b)中心波长随泵浦功率的变化

Fig. 6　Variation of pulse single. (a) Pulse duration or repetition rate versus pump power; (b) central wavelength versus pump power

4　结　　论

　　本团队采用化学气相输运法，以自下而上的路径，在云母衬底上生长碲烯纳米片。对碲烯纳米片进行表征后发现，所制备的纳米片具有较高的结晶性和环境稳定性。借助 PDMS 有机膜，结合定位转移台，实现了精准、无损的光纤集成。基于碲烯优异的非线性饱和吸收特性，在 1.55 μm 波段实现了稳定的被动调 Q 脉冲输出，中心波长约为 1558 nm，脉冲宽度约为 1.44 μs，重复频率在 87～133 kHz 范围内可调。该结果拓展了新型碲烯纳米材料的应用场景，为单质二维材料在可调谐脉冲激光器领域的应用提供了参考。

参 考 文 献

[1]　王聪，刘杰，张晗. 基于二维纳米材料的超快脉冲激光器[J]. 物理学报，2019，68(18): 188101.
　　　Wang C, Liu J, Zhang H. Ultrafast pulse lasers based on two-dimensinal nanomaterials[J]. Acta Physica Sinica, 2019, 68(18): 188101.

[2]　董自凯，宋晏蓉. 光纤激光器被动锁模技术研究进展[J]. 中国激光，2021，48(5): 0501006.
　　　Dong Z K, Song Y R. Research progress of mode-locked fiber lasers based on saturable absorbers[J]. Chinese Journal of Lasers, 2021, 48(5): 0501006.

[3]　高子叶，朱江峰，公爽，等. 基于二硫化钨可饱和吸收体双波长被动调 Q Yb: GdYSiO$_5$ 激光器[J]. 光子学报，2018，47(10): 1014002.

Gao Z Y, Zhu J F, Gong S, et al. Dual-wavelength passively Q-switched Yb∶GdYSiO$_5$ laser based on WS$_2$ saturable absorber mirror[J]. Acta Photonica Sinica, 2018, 47(10): 1014002.

[4] 王琪, 钟阳光, 赵丽云, 等. 基于二维层状材料的激光器[J]. 中国激光, 2020, 47(7): 0701008.
Wang Q, Zhong Y G, Zhao L Y, et al. Lasers based on two-dimensional layered materials[J]. Chinese Journal of Lasers, 2020, 47(7): 0701008.

[5] Li X H, An M Q, Li G, et al. MOF-derived porous dodecahedron rGO-Co$_3$O$_4$ for robust pulse generation[J]. Advanced Materials Interfaces, 2022, 9(5): 2101933.

[6] Li X H, Guo Y X, Ren Y J, et al. Narrow-bandgap materials for optoelectronics applications[J]. Frontiers of Physics, 2022, 17(1): 13304.

[7] Wang Y M, Chen Y X, Li X H, et al. Optical-intensity modulator with InSb nanosheets[J]. Applied Materials Today, 2020, 21: 100852.

[8] Zhang C X, Liu J, Gao Y, et al. Porous nickel oxide micron polyhedral particles for high-performance ultrafast photonics[J]. Optics & Laser Technology, 2022, 146: 107546.

[9] Zhang D, Zhang C X, Li X H, et al. Layered iron pyrite for ultrafast photonics application[J]. Nanophotonics, 2020, 9(8): 2515-2522.

[10] Bao Q L, Zhang H, Wang Y, et al. Atomic layer graphene as saturable absorber for ultrafast pulsed lasers[J]. Advanced Functional Materials, 2009, 19(19): 3077-3083.

[11] Loiko P A, Serres J M, Mateos X, et al. Passive Q-switching of Yb bulk lasers by a graphene saturable absorber[J]. Applied Physics B, 2016, 122(4): 105.

[12] 金雨, 杜林, 蒋国保, 等. 基于碲化铋纳米片的全光可控调 Q 光纤激光器[J]. 中国激光, 2017, 44(7): 0703014.
Jin Y, Du L, Jiang G B, et al. All-optical tunable Q-switched fiber laser based on bismuth telluride nanosheets[J]. Chinese Journal of Lasers, 2017, 44(7): 0703014.

[13] Wang T, Yu Q, Guo K, et al. Sb$_2$Te$_3$ topological insulator for 52 nm wideband tunable Yb-doped passively Q-switched fiber laser[J]. Frontiers of Information Technology & Electronic Engineering, 2021, 22(3): 287-295.

[14] 徐磊, 夏海平. 多元金属硫化物的近红外吸收性能[J]. 中国激光, 2013, 40(6): 0606001.
Xu L, Xia H P. Multi-metal sulfide for absorbing near infrared light[J]. Chinese Journal of Lasers, 2013, 40(6): 0606001.

[15] 杨闵皓, 常建华, 石少杭, 等. 新型二硫化钼可饱和吸收体的制备及其超快特性研究[J]. 中国激光, 2018, 45(10): 1001009.
Yang M H, Chang J H, Shi S H, et al. Preparation and study on the ultrafast characteristics of a new type of molybdenum disulfide saturable absorber[J]. Chinese Journal of Lasers, 2018, 45(10): 1001009.

[16] 令维军, 孙锐, 陈晨, 等. 基于反射式 MoS$_2$ 可饱和吸收体调 Q 锁模 Tm∶LuAG 激光器[J]. 中国激光, 2019, 46(8): 0808002.
Ling W J, Sun R, Chen C, et al. Passively Q-switched mode-locked Tm∶LuAG laser with reflective MoS$_2$ saturable absorber[J]. Chinese Journal of Lasers, 2019, 46(8): 0808002.

[17] 邓海芹, 樊超, 郭琨, 等. 基于斜立生长硒化铅纳米片可饱和吸收体的光纤脉冲激光研究(特邀)[J]. 光子学报, 2021, 50(10): 1014002.
Deng H Q, Fan C, Guo K, et al. Research of fiber pulse laser generation with oblique grown PbSe nanosheets saturable absorber (invited)[J]. Acta Photonica Sinica, 2021, 50(10): 1014002.

[18] Yu Q, Guo K, Dai Y P, et al. Black phosphorus for near-infrared ultrafast lasers in the spatial/temporal domain[J]. Journal of Physics. Condensed Matter, 2021, 33(50): 503001.

[19] Yu Q, Chen C, Guo K, et al. Deterministic transfer of large-scale β-phase arsenic on fiber end cap for near-infrared ultrafast pulse generation[J]. Frontiers in Materials, 2021, 8: 721587.

[20] 于静文, 王秀翊, 冯金超, 等. 锑烯纳米层片用于活体肿瘤原位光声成像[J]. 中国激光, 2020, 47(2): 0207033.
Yu J W, Wang X H, Feng J C, et al. Antimonene nanoflakes as a photoacoustic imaging contrast agent for tumor *in vivo* imaging[J]. Chinese Journal of Lasers, 2020, 47(2): 0207033.

[21] Lei T, Li J M, Lu S, et al. Electronic states driven by the crystal field in two-dimensional materials: the case of antimonene[J]. Physical Review B, 2022, 105(11): 115404.

[22] Zhao X X, Shi J W, Yin Q, et al. Controllable synthesis of high-quality two-dimensional tellurium by a facile chemical vapor transport strategy[J]. iScience, 2021, 25(1): 103594.

[23] Wang Q S, Safdar M, Xu K, et al. Van der waals epitaxy and photoresponse of hexagonal tellurium nanoplates on flexible mica sheets[J]. ACS Nano, 2014, 8(7): 7497-7505.

[24] Wang Y X, Qiu G, Wang R X, et al. Field-effect transistors made from solution-grown two-dimensional tellurene[J]. Nature Electronics, 2018, 1(4): 228-236.

[25] Guo J, Zhao J L, Huang D Z, et al. Two-dimensional tellurium-polymer membrane for ultrafast photonics[J]. Nanoscale, 2019, 11(13): 6235-6242.

[26] Liu G W, Yuan J J, Wu T G, et al. Ultrathin 2D nonlayered tellurene nanosheets as saturable absorber for picosecond pulse generation in all-fiber lasers[J]. IEEE Journal of Selected Topics in Quantum Electronics, 2021, 27(2): 0900106.

[27] Calavalle F, Suárez-Rodríguez M, Martín-García B, et al. Gate-tuneable and chirality-dependent charge-to-spin conversion in tellurium nanowires[J]. Nature Materials, 2022, 21(5): 526-532.

[28] 龚甜. 二维对称碲烯生长机理及性能研究[D]. 武汉: 湖北大学, 2021: 1-74.
Gong T. Study on the growth mechanism and the properties of two-dimensional symmetric tellurene[D]. Wuhan: Hubei University, 2021: 1-74.

[29] Chen J, Wang J, Yu Q, et al. Sub-band gap absorption and optical nonlinear response of MnPSe$_3$ nanosheets for pulse generation in the L-band[J]. ACS Applied Materials & Interfaces, 2021, 13(11): 13524-13533.

[30] Yu Q, Wang S, Zhang Y, et al. Femtosecond ultrafast pulse generation with high-quality 2H-TaS$_2$ nanosheets *via* top-down empirical approach[J]. Nanoscale, 2021, 13(48): 20471-20480.

[31] Akbari R, Zhao H, Fedorova K A, et al. Quantum-dot saturable absorber and Kerr-lens mode-locked Yb∶KGW laser with > 450 kW of peak power[J]. Optics Letters, 2016, 41(16): 3771-3774.

Chemical Vapor Transport Grown Tellurium Nanoflakes for Infrared Pulse Generation

Pang Xiuyang[1], Zhao Xinxin[2], Yu Qiang[1*], Deng Haiqin[1], Liu Fangqi[3], Zhang Yan[2],
Shu Bowang[1], Xian Tianhao[4], Zhu Sicong[3], Wu Jian[1], Hou Yifeng[5], Zhang Kai[2**], Jiang Zongfu[1]

[1]*College of Advanced Interdisciplinary Studies, State Key Laboratory of Pulsed Power Laser Technology, Hunan Provincial Key Laboratory of High Energy Laser Technology, National University of Defense Technology, Changsha 410073, Hunan, China;*

[2]*i-Lab & Key Laboratory of Nanodevices and Applications, Key Laboratory of Nanophotonic Materials and Devices, Suzhou Institute of Nano-Tech and Nano-Bionics, Chinese Academy of Sciences, Suzhou 215123, Jiangsu, China;*

[3]*The State Key Laboratory for Refractories and Metallurgy, Wuhan University of Science and Technology, Wuhan 430081, Hubei, China;*

[4]*School of Physics and Astronomy, Shanghai Jiao Tong University, Shanghai 200240, China;*

[5]*College of Electronical and Information Engineering, Wuzhou University, Wuzhou 543001, Guangxi, China*

Abstract

Objective In recent years, low-dimensional materials have received significant attention in optics and demonstrated excellent application prospects. In the previous studies, numerous carbon, nitrogen, and oxygen group single element films, such as arsenic, antimony, and tellurium, have been obtained. Tellurene is a basic material of the oxygen group with a helical chain structure. It may form various morphologies, such as nanowires, nanorods, nanotubes, or nanoribbons. On the one hand, preparing a thin layer of single tellurene crystal remains a challenge. On the other hand, as one of the chalcogenide elements (group VI materials), tellurene is a promising material for infrared optical applications because of its wideband absorption, high mobility, and unique topological properties. The electrical and topological properties of tellurene single crystals have been systematically studied. A second harmonic property in the optical nonlinear characteristics has also been observed. However, nonlinear applications, especially an ultrafast pulsed fiber laser based on the saturable absorption of tellurene, require further studies. In the present study, tellurene nanoflakes with high crystallinity were prepared by adopting the chemical vapor transport method. Using the precise transfer technology, the tellurium nanoflakes were integrated into the tip of the optical fiber as fiber-compatible saturable absorbers. The nonlinear saturation absorption property enabled achieving stable passively Q-switched laser pulses. It is envisaged that the present work will extend the range of applications of novel tellurene nanomaterials and provide a potential means of obtaining tunable pulsed lasers.

Methods A tellurene-based saturable absorber was prepared using a bottom-up approach and then used for laser pulse generation. Firstly, tellurium powder and mica substrate were placed on each side of the middle-necked quartz tube. The quartz tube was sealed under vacuum and then placed in a double temperature zone furnace. By executing an appropriate temperature program, the source material was vaporized, transported, and recrystallized. The as-grown nanoflakes were characterized using optical microscope, atomic force microscope, electron microscope, and a Raman spectrometer. Then, the tellurium nanoflakes were integrated into the tip of the optical fiber as fiber-compatible saturable absorbers using our polydimethylsiloxane (PDMS)-assisted accurate transfer method. Finally, the fiber-compatible saturable absorbers were integrated into an in-house erbium-doped fiber laser ring cavity for laser pulse generation.

Results and Discussions Tellurene nanoflakes were prepared using a bottom-up approach and then comprehensively characterized. The thickness of the as-grown tellurene nanoflakes was about tens of nanometers and the maximum transverse size was 80 μm. The E_1 (transverse to mode), A_1, and E_2 active Raman phonon modes of tellurium were found consistent with their typical characteristic peaks reported previously. The characteristic crystal plane is consistent with the PDF card (JCPDS ♯ 36-1452). Furthermore, the high-resolution transmission electron microscopy image showed a clear atomic image. The prepared tellurene nanoflakes have high elemental purity. All characterization methods confirmed that the tellurene nanoflakes have high crystalline quality. The saturated absorption characteristic was studied with a double arm detection system. By fitting the saturable absorption curve to the data, the modulation depth, saturation strength, and unsaturated loss were found to be 0.5%, 0.66 GW/cm², and 99.16%, respectively. Benefiting from the excellent nonlinear saturation absorption property of tellurene, a stable passively Q-switched laser was realized. The Q-switched pulses are achieved at a communication band with a center wavelength of ～1558 nm and pulse duration of 1.44 μs, and the repetition frequency is adjustable from 87 to 133 kHz. Additionally, the signal-to-noise ratio is ～53.96 dB, indicating good pulse stability. The reported results point out a potential way to achieve tunable pulsed lasers.

Conclusions Tellurene nanoflakes have been prepared using a bottom-up approach adopting chemical vapor transport. After comprehensive physical and chemical characterization, it was confirmed that the tellurene nanoflakes had a high crystallinity and

environmental stability. The nanoflakes were transferred using the PDMS‑assisted dry transfer method onto the end cap of the optical fiber with a high coverage over the core area. Benefiting from the nonlinear saturation absorption property of tellurene, stable passive Q‑switched laser pulses were achieved in the communication band with a center wavelength of 1558 nm and pulse duration of 1.44 μs. The repetition frequency was adjustable from 87 to 133 kHz. The results extend the application scenarios of novel tellurene nanomaterials and provide a potential pathway to obtaining tunable pulsed lasers.

Key words   lasers; nanomaterials; saturable absorber; passively Q‑switching; tunable pulse laser; tellurene